

DNA-linked metal nanosphere materials: Fourier-transform solutions for the optical response

A. A. Lazarides and G. C. Schatz

Department of Chemistry, Northwestern University, Evanston, Illinois 60208-3113

(Received 18 October 1999; accepted 15 November 1999)

Methods are developed for modeling the optical properties of aggregates of large numbers of small metal nanospheres in a dielectric medium. Aggregates are modeled as systems of coupled dipoles, with the dipole polarizabilities for the spheres determined using Mie theory. Fast-Fourier-transform (FFT) and conjugate-gradient (CG) techniques are used to solve the electrodynamic equations for both ordered and disordered aggregates. Results are shown to match solutions arrived at by direct methods. The range of validity of the coupled-dipole approximation for modeling DNA-linked colloidal materials is established by comparison with coupled-multipole results. While the methods are applicable only to lattice gas aggregates and aggregates composed of nanospheres on cubic lattices, there are no restrictions as to aggregate shape. © 2000 American Institute of Physics.

[S0021-9606(00)52006-6]

I. INTRODUCTION

Recent developments in the design of nanoparticle-based materials have yielded nanostructured materials with distinctive properties. Among the new synthetic strategies is that of DNA-driven assembly of colloidal nanoparticle aggregates.¹ Gold spheres, for example, coated with thiol-capped oligonucleotides are exposed to free oligonucleotide, one end of which is complementary to the DNA on half of the nanoparticles, the other end of which is complementary to the DNA on the rest of the nanoparticles. DNA hybridization pulls the nanoparticles together and yields a reversibly aggregated dielectric material whose optical properties differ significantly from those of noninteracting, dispersed particles and also from those of fractal colloidal aggregates formed through irreversible kinetic processes.²

To model the optical properties of the aggregates, one must describe the electrodynamic response of a large number of rather closely packed nanospheres. Whereas the response of a single sphere is easily described as a superposition of electric and magnetic multipoles of various orders and the response of a small number of nanospheres can be determined by self-consistent solution of the coupled multipole equations, collections of nanoparticles of the numbers ($> 10^3$) observed in DNA-linked colloidal networks are impossible to model using direct methods that scale prohibitively with particle number. While ultimately it may prove reasonable to discard explicit particle models in favor of effective medium models, we use explicit models here so that details of the dependence of optical properties on internal structure can be reliably determined.

While the DNA-linked system presents a problem of scale, it has some distinctive structural properties that simplify the modeling problem. The DNA coating provides an exclusion layer that separates the nanoparticles by a few nanometers. DNA hybridization, while energetically favored, is reversible,¹ and mild annealing produces aggregates with fairly uniform metal density, as observed by transmission

electron microscopy.³ Ordering is energetically favored and has been observed for modest length scales through small-angle x-ray scattering.⁴ The division of the nanospheres into two species on the basis of their oligonucleotide coating leads to structures that are topologically binary. Structures that allow particles to have a large number of complementary nearest neighbors are preferred over the face-centered-cubic, hexagonal close-packed, and random close-packed structures that can form when particles interact nonspecifically.⁵

We have developed methods for modeling the electrodynamic response of large arrays (up to 10^5) of small coupled metal nanospheres. Here we describe an explicit particle model in which each nanosphere is modeled as a dipole responding to a local field composed of the incident field and the retarded fields of the other nanoparticles. Higher order response is neglected because, in the DNA-linked aggregates, the oligonucleotide layer maintains interparticle separations that are large enough to render short-range high-order effects small. We adopt efficient methods of solving coupled electrodynamic equations⁶ so as to be able to model aggregates composed of a number of particles sufficient to display the optical properties of the DNA-linked material.

In Sec. II we describe an interacting dipole model for electrostatically coupled spheres and outline a method for efficient solution of the coupled equations based upon conjugate-gradient (CG) and fast-Fourier-transform (FFT) methods. In Sec. III we demonstrate that the solutions produced using the CG/FFT method are the same as the solutions produced using slower direct methods. In Sec. IV we explore the range of validity of the coupled-dipole approximation for ordered and disordered arrays of 13 nm gold spheres. In Sec. V we summarize the properties of DNA-linked nanoparticle materials that led us to develop the methods described here. In the final section, we discuss the applicability of the methods to other materials.

II. ELECTRODYNAMIC THEORY FOR AGGREGATES

A. Coupled nanospheres

The behavior of light incident on a macroscopic target is governed by Maxwell's equations for the electric and magnetic vector fields. The general framework for modeling the optical response of a collection of spheres involves a self-consistent solution of the response of each particle to the incident field and the scattered fields of the other particles. The response of individual spheres to the local field can be determined by decomposing the local field into vector spherical harmonics and evaluating the response to each partial wave.^{7,8} Mie⁹ solved the problem for dilute collections of spheres by deriving the plane wave response of an isolated sphere. Spherical particles of nonmagnetic materials with sizes much smaller than the wavelength of light respond primarily to the electric dipole component of the local field. For isotropic materials, the frequency-dependent dipole polarizability, α_1 , is a scalar and is determined by the electric dipole scattering coefficient, a_1 ,¹⁰ according to the expression¹¹

$$\alpha_1 = r^3 \frac{3i}{2(kr)^3} a_1, \quad (1)$$

where r is the sphere radius, $k = m_0(2\pi/\lambda)$ is the magnitude of the wavevector in a dielectric medium with real refractive index, m_0 , and a_1 is a function of the size parameter, kr , and relative metal index of refraction, $m = \sqrt{\epsilon}/m_0$. For very small spheres, the bulk dielectric function must be corrected¹² for scattering from the sphere surface (quantum size effect). Because, for these small spheres, the response to higher-order components of the field is so small, rather dense collections of spheres are well defined by their dipole response.

Therefore, except when the component nanospheres are very closely spaced (and higher than dipole components of the local field become extremely large), the response of an aggregate to electromagnetic radiation can be determined by a self-consistent solution of the electric dipole polarizations, \mathbf{P}_i , of each sphere in the superposed field of the incident light and the dipole fields of the other particles. For a given dipole at position, \mathbf{r}_i ,

$$\mathbf{P}_i = \alpha \cdot \mathbf{E}_{\text{loc}}(\mathbf{r}_i), \quad (2)$$

where $\mathbf{E}_{\text{loc}}(\mathbf{r}_i)$ is the sum of the incident plane wave, $\mathbf{E}_{\text{inc},i} = \mathbf{E}_0 \exp(i\mathbf{k} \cdot \mathbf{r}_i - i\omega t)$ and the retarded fields

$$-\mathbf{A}_{ij} \cdot \mathbf{P}_j = \frac{e^{ikr_{ij}}}{r_{ij}^3} \left\{ k^2 \mathbf{r}_{ij} \times (\mathbf{r}_{ij} \times \mathbf{P}_j) + \frac{1 - ikr_{ij}}{r_{ij}^2} \times [r_{ij}^2 \mathbf{P}_j - 3\mathbf{r}_{ij}(\mathbf{r}_{ij} \cdot \mathbf{P}_j)] \right\}, \quad (3)$$

of the other $N-1$ dipoles, and α is a polarizability tensor with elements $\alpha_{kl} = \delta_{kl}\alpha_1$. The dipole fields at location i depend upon the dipoles, \mathbf{P}_j , as a function of the displacements, $\mathbf{r}_{ij} = \mathbf{r}_i - \mathbf{r}_j$, between locations i and j . Use of the

retarded field expression eliminates the need for explicit modeling of the time dependence of the fields and polarizations. Thus,

$$(\alpha^{-1})\mathbf{P}_i + \sum_{j \neq i} \mathbf{A}_{ij} \cdot \mathbf{P}_j = \mathbf{E}_{\text{inc},i}. \quad (4)$$

The N linear complex equations for 3-vectors \mathbf{P}_i and $\mathbf{E}_{\text{inc},i}$ can be formulated as a single $3N$ -dimensional matrix equation,

$$\mathbf{A}\mathbf{P} = \mathbf{E}_{\text{inc}}, \quad (5)$$

where \mathbf{P} and \mathbf{E}_{inc} are $3N$ vectors and \mathbf{A} is a $3N \times 3N$ symmetric matrix constructed from the 3×3 interparticle interaction matrices \mathbf{A}_{ij} , with additional terms, α_1^{-1} , along the diagonal. Higher multipole couplings could also be included. However, as we illustrate in Sec. IV, for aggregates composed of fairly uniformly packed small spheres separated by distances that are substantial relative to the particle diameter, they are not needed.

B. Iterative conjugate-gradient and fast-Fourier-transform solution

Direct inversion of Eq. (5) is time consuming for targets with large numbers, N , of spheres, since the computation associated with the matrix inversion scales as N^3 . Storage requirements for the full $(3N \times 3N)$ complex matrix, \mathbf{A} , may also be prohibitive. Fortunately, an alternative approach adopted for solution of a finite element form of the free-space single particle scattering and absorption problem¹³ is applicable to the many particle coupled dipole problem. Following Draine,¹⁴ we use a special case of the conjugate-gradient (CG) scheme described by Petravic and Kuo¹⁵, to solve Eq. (5) by iteration. Successive estimates of the polarization vector, \mathbf{P} , are made by incrementing the prior estimate through addition of a vector that is \mathbf{A} -conjugate to all earlier increments. The CG algorithm requires evaluation of matrix-vector products of the form $\mathbf{A}\mathbf{X}$ and $\mathbf{A}^\dagger\mathbf{X}$, (where the \mathbf{X} are vectors of position-dependent 3-tuples) but not the individual components of the interaction matrix, \mathbf{A} . Because the elements of the interaction matrix depend only upon the interparticle vectors, r_{ij} , and not the individual particle positions, for a collection of particles on a lattice, each element of the vector, $\mathbf{A}\mathbf{X}$, is a discretized convolution. The lattice is doubled in each dimension so that \mathbf{A} and \mathbf{X} can be regarded as periodic, and the matrix-vector products are evaluated by multiplication of their discrete Fourier transforms. As in Ref. 6, we use a fast-Fourier-transform (FFT) technique¹⁶ to speed the calculation of the matrix-vector products, thereby reducing the scaling of the computation from $O(N^2)$ to between $O(N_L \ln(N_L))$ and $O(N_L^{4/3})$ where N_L is the number of lattice sites in a rectangular volume containing the occupied sites. The specific FFT algorithm is that of Brenner¹⁷ as implemented in the DDSCAT code of Goodman, Draine, and Flatau.⁶ Use of the FFT technique restricts particles to lattice locations. Our method is restricted therefore to ordered nanoparticle aggregates and disordered aggregates of the lattice gas variety. The gain in efficiency is greatest for nanospheres arrayed on simple cubic lattices. For nanospheres on a bcc

lattice, N_L is at least $4N$, as within the aggregate boundary only one quarter of the sites of the simple cubic lattice on which the bcc array is constructed are occupied. The method imposes no restrictions on aggregate shape, and size constraints follow only from the aforementioned scaling of computation with particle number.

C. Optical cross sections

Once the polarizations, P_j , are known, the extinction cross section is computed using the expression¹⁴

$$C_{\text{ext}} = \frac{4\pi k}{|E_{\text{incl}}|^2} \sum_{j=1}^N \text{Im}\{E_{\text{inc},j}^* \cdot P_j\}. \quad (6)$$

Each term provides the formal contribution of one particle to the forward scattering and, by means of the optical theorem, to the aggregate extinction. Absorption is calculated as

$$C_{\text{abs}} = \frac{4\pi k}{|E_{\text{incl}}|^2} \sum_{j=1}^N \left\{ \text{Im}\{P_j \cdot (\alpha_j^{-1})^* P_j^*\} - \frac{2}{3}k^3 P_j \cdot P_j^* \right\}, \quad (7)$$

and scattering as the difference, $C_{\text{sca}} = C_{\text{ext}} - C_{\text{abs}}$.

III. VALIDATION OF THE FOURIER-TRANSFORM TECHNIQUE

The fast-Fourier transform iterative conjugate-gradient (CG/FFT) solution for aggregate particle polarizations was tested by comparing the extinction spectra determined for particular model aggregates using polarizations calculated with both direct and Fourier-transform methods. All aggregates are composed of 13 nm gold spheres embedded in a dielectric medium with the dielectric constant of water. Calculations were performed using gold dielectric functions from the literature.^{18–21}

Figure 1 displays extinction spectra for aggregates at the upper limits of density for colloid on a given lattice. Extinction spectra for a simple cubic (sc) array of 552 13 nm spheres forming a 132 nm spherical aggregate are illustrated in Fig. 1(a). The colloid volume fraction is 0.52, which corresponds to a lattice parameter equal to the particle diameter. The dashed line is the extinction spectrum based on polarizations calculated using the iterative CG/FFT solution of Eq. (5). The solid line is the spectrum calculated using polarizations determined by direct solution of Eq. (5). The two spectra are almost identical.

Figure 1(b) compares spectra for a body-centered-cubic (bcc) array of spheres arranged into a 118 nm spherical aggregate. As in Fig. 1(a), the colloid volume fraction is the upper limit for the given lattice, which for bcc is 0.68. As in Fig. 1(a), the CG/FFT calculation yields the same spectrum as the direct calculation. The matching of Fourier-transform and direct solutions was achieved also for aggregates with lower colloid fractions that correspond to the fractions occurring in DNA-linked materials and for which the coupled-dipole approximation is accurate.

The constraint that particles be located on a cubic grid, which is necessary for accurate representation of interparticle interactions in Fourier space, does not impose any restriction on the occupation of the lattice. Substitutional disorder, such

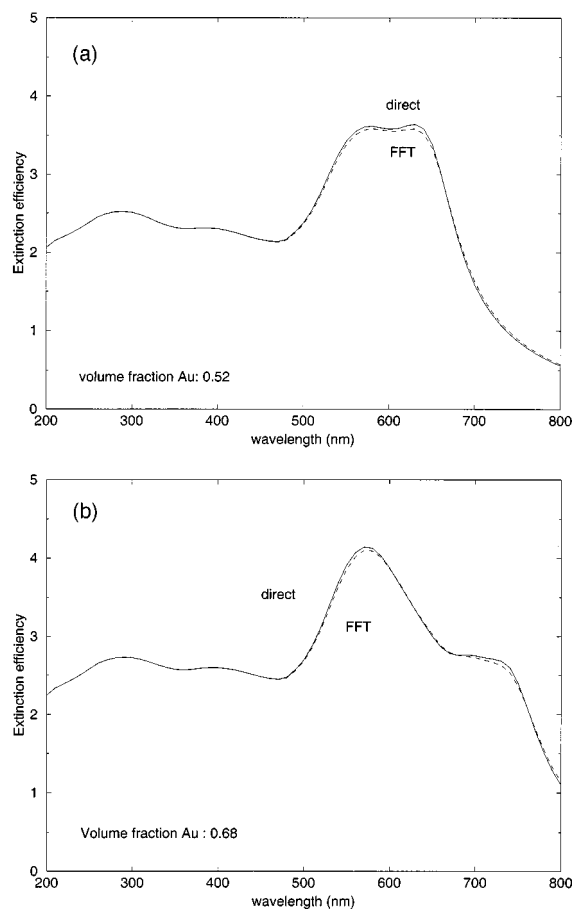


FIG. 1. (a) Extinction spectra calculated for a 132 nm spherical aggregate of 13 nm gold spheres in a simple cubic array in water. Solid line represents direct solution; dashed line is Fourier-transform solution. (b) Same as (a) for a 118 nm spherical aggregate with a bcc structure.

as that of a lattice gas, does not preclude Fourier-space solution of the polarization response. This was demonstrated by comparing extinction spectra for substitutionally disordered targets calculated using the FFT algorithm with spectra calculated from polarizations determined by a direct solution of Eq. (5). Spectra for a disordered 156 nm target with gold volume fraction 0.2 are displayed in Fig. 2. The aggregate

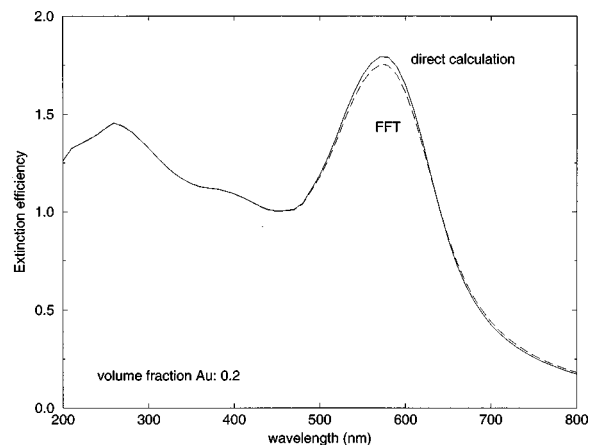


FIG. 2. Extinction spectra calculated for a disordered 156 nm spherical aggregate of 13 nm gold spheres in water. Solid/dashed lines as in Fig. 1.

model was generated from a defect-free bcc array by random deletion of 895 of the original 1243 spheres. As with the defect-free targets, the FFT solution reproduces the direct solution.

Significant variation among the plasmon properties of the various aggregates can be seen by comparing the spectra in Figs. 1 and 2. Using an alternative theoretical treatment, we show elsewhere²² that the various features involve magnetic as well as electric dipole contributions to the plasmon spectra. The aggregate-size and colloid-fraction dependence of the collective electronic response is also considered in Ref. 23.

IV. VALIDITY OF THE SINGLE DIPOLE APPROXIMATION

The exact solution for the extinction of a sphere in a plane wave field is given by Mie theory.⁹ At wavelengths for which the product, $|m|kr$, of the size parameter, kr , and the relative refractive index, m , is much less than one, the extinction of an isolated sphere is accurately approximated by the electric dipole term, i.e., the first term in the spherical harmonic expansion from which the Mie result is constructed. For gold spheres in water, the electric dipole description of the optical response is quite accurate throughout the visible range, for spheres 30 nm or smaller in diameter. In the plasmon region, spheres as large as 100 nm are reasonably well modeled as dipoles. (Larger spheres approach or exceed the Rayleigh limit, $kr \approx 1$, and require higher-order interaction models.) However, a nanosphere in an aggregate experiences an incident field which is not a plane wave field by virtue of the modulation of that field by the other particles in the aggregate. When the separation between particles is large, only the dipole fields are significant. When the particles are close together, the higher-order multipole components of the local field become important. For a given nanosphere size and material and a given dielectric medium, there is a lower limit to the interparticle spacings for which the dipole approximation for nanospheres gives accurate visible extinction spectra for the composite material. In this section we examine the validity of the dipole approximation for modeling the extinction of aggregates of gold nanospheres in water.

A. Comparison of dipole calculations with exact theory

The interacting dipole model was evaluated by comparing dipole calculations with calculations in which the nanosphere response was modeled using as many multipoles as required to obtain convergence of the aggregate extinction for a range of wavelengths spanning the UV-visible spectrum. The calculations were performed using T -matrix methods²⁴ developed by Mackowski and Mishenko for clusters of spheres. An aggregate T -matrix with an aggregate-centered spherical harmonic basis is constructed from transformed single particle T -matrices. An orientation-averaged extinction spectrum is calculated from the aggregate T -matrix at each wavelength. While the method is efficient for compact aggregates and particularly for spherical aggregates (because their response is accurately described by a

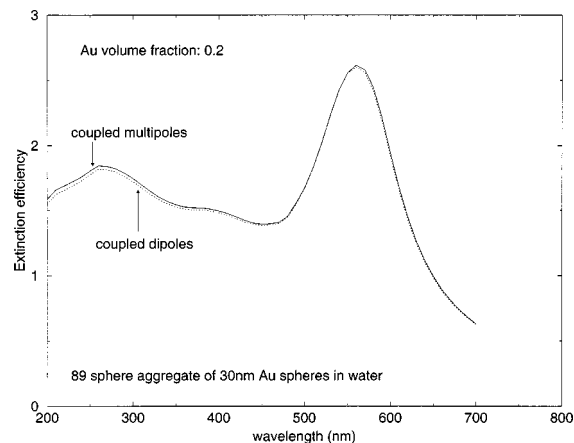


FIG. 3. Extinction spectra for a spherical aggregate of 89 30 nm Au nanospheres in water. The aggregate is 230 nm in diameter. The spheres are arranged in a bcc array with 15 nm between nearest neighbors. Dotted line (\cdots) is the spectrum calculated using an interacting dipole model of the coupled spheres. Solid line ($—$) is the coupled multipole solution.

relatively low-order spherical harmonic expansion), the scaling of the computation with particle number is sufficiently high order in particle number that we restrict our comparisons to aggregates of less than 100 particles. All calculations described here are for gold nanoparticles in water.

Initially, we compared dipole and multipole calculations for ordered arrays of 30 nm gold nanospheres in water. Among approximately spherical aggregates with bcc structure, a small fraction are particularly spherical by virtue of having a filled shell of surface particles. Among these is an 89 sphere aggregate. Figure 3 displays extinction spectra for a 230 nm spherical aggregate composed of 89 spheres with separations of 15 nm (a radius) between spheres. The aggregate is 20% Au by volume and the aqueous medium is modeled using a dielectric constant of 1.77. The extinction efficiencies are averaged over all aggregate orientations relative to the propagation direction of the incident radiation. In the UV (where the particle size parameter, kr , is greater than 0.4, and mkr , is somewhat larger), the extinction is underestimated slightly when only the dipole interaction is included. In the visible range (where kr is less than 0.4, but $|m| > 1$), the dipole calculation closely matches the multipole calculation and accurately reproduces the plasmon peak, which is redshifted 35 nm from the plasmon of dispersed aqueous 30 nm Au spheres ($\lambda_{\text{peak}} = 527$ nm). The dipole calculation is thus quite accurate for space-filling aggregates of spheres when the sphere size is below the Rayleigh limit and the particles are separated by a radius.

The accuracy of the coupled-dipole approximation, however, varies with interparticle spacing. To determine the range of spacings for which the coupled-dipole description accurately represents the optical response of ordered Au nanoparticle aggregates, we calculated extinction spectra for denser versions of the 89-sphere aggregate, again using both coupled-multipole and coupled-dipole methods. The calculated plasmon peak shifts for these aggregates are plotted in Fig. 4. For particle separations of $0.8r$, $0.6r$, and $0.4r$ (Au volume fractions 0.25, 0.31, and 0.39), the wavelength of the aggregate extinction maximum is redshifted 46.5, 65.5, and

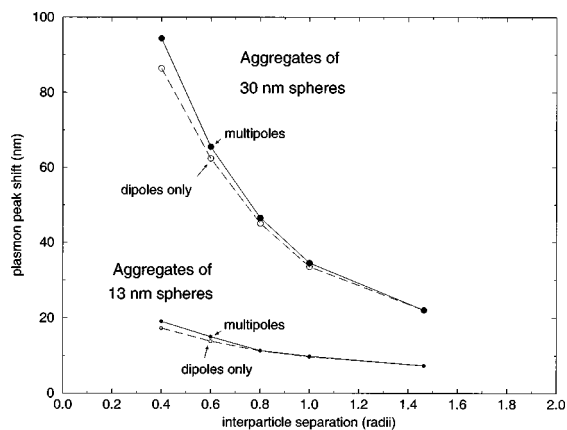


FIG. 4. Plasmon peak shifts associated with formation of an 89-sphere aggregate of 30 or 13 nm Au spheres as a function of the radius-normalized interparticle separation (s/r) within the aggregate. Exact peak shifts are identified using filled circles. Peak shifts determined using approximate calculations in which the intersphere couplings are approximated as dipole-dipole interactions are identified using open circles. The spherical aggregates are composed of nanospheres arranged on a bcc lattice. The medium has a dielectric constant of 1.77. Au volume fraction varies from 0.39 (for $s/r=0.4$) to 0.13 ($s/r=1.45$).

94.4 nm, respectively, from the dispersed particle plasmon peak. The dipole calculations underestimate the peak shifts by 3%, 5%, and 8%, respectively. As expected, the accuracy of the coupled-dipole approximation decreases as the interparticle spacing decreases. However, the error growth is quite gradual, and the error in the plasmon peak shift is less than 10% for spacings as small as $0.4r$. For 1% accuracy in the plasmon peak location at this spacing, poles up to hexadecapole must be included in the description of each 30 nm Au sphere.

The scaling of the accuracy of the dipole approximation with particle size was investigated by repeating the particle-spacing dependent analysis with aggregates of smaller spheres. Extinction spectra were calculated at both the dipole and multipole levels for an 89 sphere aggregate of 13 nm spheres for a variety of particle separations. The plasmon peak shifts of the small-sphere aggregates as a function of radius-normalized interparticle separation are plotted in Fig. 4 (below the results for aggregates of 30 nm particles) and listed in Table I. As for the aggregates of 30 nm spheres, two sets of peak shifts are shown in Fig. 4, one calculated using a full interaction model, and the other based on the coupled-dipole approximation. The coupled-dipole results for the plasmon peak location are accurate to within 1% for particles separated by $0.8r$ (5.4 nm) or more, but underestimate the peak shifts by 6% and 9% when the particle separations drop to $0.6r$ and $0.4r$ (3.9 and 2.6 nm), respectively. Thus, while the relative peak shift errors for spherical aggregates of 13 nm spheres are smaller than those for aggregates of 30 nm spheres at spacings less than or equal to $0.8r$, at smaller spacings the relative errors are comparable for aggregates of particles of either size when the Au volume fraction is the same.

The success with which ordered aggregates composed of closely spaced nanospheres are modeled as coupled dipoles cannot be assumed to carry over to disordered aggregates. In

TABLE I. Errors associated with use of the dipole approximation in the location of the plasmon peak extinction for spherical aggregates of 89 13 nm Au spheres as a function of minimum interparticle spacing. Peak shifts are relative to the wavelength (525 nm) of the plasmon peak of an isolated 13 nm sphere. All calculations are for particles in a medium with dielectric constant 1.77. Accurate peak shifts are calculated using a multipole description of the particle polarizations and fields. Peak shift errors are differences between results of dipole and multipole calculations, expressed as a percentage of the accurate (multipole) peak shifts. Among aggregates with the same number of particles and the same minimum interparticle separation, disordered arrays are larger and have lower metal fraction than ordered arrays.

Interparticle spacing	Au volume fraction	Plasmon peak shift	Shift error using dipoles
Ordered arrays			
9.5 nm ($1.46r$)	0.13	7.3 nm	...
6.5 nm ($1.0r$)	0.20	9.5 nm	0.9%
5.4 nm ($0.82r$)	0.25	11.3 nm	1%
4.0 nm ($0.6r$)	0.31	15. nm	6%
2.8 nm ($0.4r$)	0.39	19. nm	9%
Disordered arrays			
5.0 nm ($0.78r$)	0.20	11.5 nm	7%
4.0 nm ($0.6r$)	0.20	13.6 nm	14%
2.8 nm ($0.4r$)	0.20	17.8 nm	19%

disordered arrays, the fields vary from particle location to particle location as a function of the local microstructure and fluctuations in the polarizations of nearby particles. We observe, however, that lattice-gas aggregates of spheres (aggregates modeled as spheres arrayed on a lattice with random vacancies) require higher-order interaction models if and only if the minimum sphere separation is a small fraction of the particle size. Our conclusion is based upon an evaluation of the error associated with neglect of higher-than-dipole interactions for several disordered arrays of gold spheres in water. For comparison with the ordered aggregates discussed above, we again used 89-sphere aggregates of 13 nm spheres. The disordered aggregates have vacancy levels varying from 0.21 to 0.47, but identical Au volume fractions (0.2). In a given aggregate, the minimum spacing between particles is characteristic of the defect-free bcc lattice from which the vacancy structure was derived. As in our evaluation of dipole modeling of ordered aggregates, extinction spectra calculated using the coupled dipole model were compared with spectra calculated using all higher-order interactions necessary to converge the spectra. Results are presented in the lower half of Table I for three arrays, with minimum separations varying from $0.8r$ to $0.4r$. While these aggregates have lower metal fraction than ordered arrays with the same minimum separation, the plasmon peak shifts are close to those of smaller, ordered arrays with the same number of nanoparticles and same minimum separation.

As with ordered aggregates, the errors associated with neglect of high-order interaction grow as the spacing between nearest-neighbor particles decreases. The fractional error in the plasmon peak location relative to that of unaggregated colloid is negligible for arrays in which the sphere separation is greater than a particle radius, but grows to 7% for spheres separated by $0.8r$, 14% for spheres separated by $0.6r$, and 19% for spheres separated by $0.4r$. Thus, for disordered aggregates, the fractional errors associated with ne-

glected interaction orders are more than twice as large as the errors (1, 6, and 9%) observed for ordered aggregates with the same particle separation, as documented in Table I, even though the plasmon shifts themselves are comparable when the minimum separations are the same. When compared with the error (<1%) for an ordered array with the same metal volume fraction (0.2), the errors associated with dipole modeling of substantially disordered arrays are more than an order of magnitude larger. Thus, while the correspondence between errors in ordered and disordered arrays is weak, the importance of including higher-order interactions in models of lattice-gas aggregates appears to correlate more closely with minimum separation than with metal fraction. This is a reasonable consequence of the distance dependence of the various interaction orders, dipole interactions being long-ranged and higher-order interactions increasingly short-ranged.

B. Discussion

From these comparisons we conclude that the optical extinction of spherical aggregates of small gold nanoparticles is accurately represented using coupled-dipole interactions when the particles are separated by a substantial fraction of a particle radius. The lower limit for nearest neighbor separations that keeps plasmon shift errors below 10% is $0.4r$ for ordered arrays. For disordered arrays errors develop at larger separations. In the examples examined here, 10% errors are characteristic of disordered arrays with minimum separations of approximately $0.7r$. Below these limits, higher-order multipoles induce significant additional polarizations in their nearest neighbors.

The accuracy of the dipole description of DNA-linked nanoparticle networks is dependent, therefore, on the interparticle separations enforced by the oligonucleotide coating. X-ray diffraction data⁴ collected at small angles for linked 14 nm particles indicates a center-to-center distance of 20.5 nm, corresponding to a separation of $0.93r$, for the shortest (24 base pair) standard linker. The dipole model can thus be expected to provide a more or less accurate description of the plasmon peak location depending on the range of order of the linked material, with an error of a few percent for the most disordered material.

Other theoretical studies^{25–27} of the dielectric properties of disordered metal dielectric composites have revealed the simplification of the interparticle interaction that derives from the presence of an exclusion region around each particle. Prior to these, Lamb, Wood, and Ashcroft²⁸ discussed, conversely, that multipole effects in low inclusion fraction, disordered systems of unprotected particles derive from the occurrence of closely approaching particles within the material.

Because our primary interest is in three-dimensional aggregates, we have not explored the accuracy of the dipole approximation for lower-dimensional structures. However, at the level of electrostatics, this has been done by Claro²⁹ who found that the coupled-dipole description of infinite 1D and 2D arrays is comparably accurate to that of 3D arrays. In contrast, in those few-particle arrays where quadrupole excitations do couple strongly to the dipole response, inaccura-

cies appear in dipole models at separations larger than the separations found to be critical for dipole models of extended structures. Electrodynamic analyses of silver nanoparticles³⁰ confirm the importance of higher-order couplings for pairs of particles with edge-to-edge separations less than one radius.

V. APPROPRIATENESS OF THE METHOD FOR MODELING DNA-LINKED ASSEMBLIES

The large aggregate calculations described here use CG/FFT methods to solve the coupled-sphere problem at the coupled-dipole level. The methods were chosen because they efficiently provide accurate descriptions of the linear optical response of DNA-linked nanosphere materials. Although the DNA-linked materials have substantial metal fractions, they possess properties that greatly reduce the complexity of interactions between component particles. Firstly, the gold nanoparticles are much smaller than visible wavelengths (300–700 nm). Secondly, the DNA coating separates particles of the standard size (12–16 nm) by distances on the order of a particle radius. Thirdly, because DNA hybridization is not only energetically favored but also reversible, annealing drives the network materials to ordered structures that maximize the number of DNA links. Even when disorder is present (e.g., when aggregates are formed at temperatures significantly below the melting temperature, or annealing results in only short range order), the DNA exclusion layer greatly constrains the magnitude of the effects of disorder on interparticle interactions. The combined effect of small particle size, substantial particle separations, and uniform density eliminate the need to model interactions higher in order than the dipole interactions modeled here.

The use of two groups of nanoparticles each with a different oligonucleotide coating facilitates the modeling in another way. When aggregates are formed by sequence-specific hybridization that links particles functionalized with one oligonucleotide only to particles functionalized with a different oligonucleotide, binary structures are formed. Body-centered-cubic structures, which among binary structures have the highest nearest-neighbor number (8) and, therefore, the largest number of DNA links per particle, are favored. Close-packed structures, which provide an average of six complementary nearest neighbors are disfavored. The exclusion of hexagonal close-packed and random close-packed structures allows for the use of methods that are applicable only to cubic lattice materials.

VI. CONCLUSION

We have demonstrated that efficient conjugate-gradient and fast-Fourier-transform methods can be used to calculate the optical response for large aggregates of small nanospheres. While CG/FFT methods are used routinely in electromagnetics,³¹ and have recently been used to model the scattering of grains in space,⁶ we are not aware of their use in models of composite media. Use of the CG/FFT method greatly reduces the computational and memory requirements of the coupled particle problem.

In this work we use CG/FFT methods to solve the coupled-sphere problem at the coupled-dipole level. While the method could be extended to include higher-order interactions in the intersphere coupling, the added complexity appears not to be warranted for the DNA-linked nanosphere materials in which we are interested.

Because the validity of our simple modeling scheme is a consequence of the special properties of materials assembled with DNA-direction, the approach is not directly extendable to many other materials. Particles that interact nonspecifically and bind irreversibly typically form fractal aggregates² that lack the properties that render dipole models accurate for DNA-linked materials. For these other materials, coupled-dipole models that use single particle polarizabilities derived from Mie theory³² are only accurate if the particles themselves are of materials that have low levels of polarizability at the frequencies of interest. Reasonable accuracy can be achieved for fractal aggregates of metal particles with a coupled dipole treatment only by replacing the single particle polarizability derived from Mie theory with alternative dipole polarizabilities that take into account the higher-order interactions, or otherwise renormalizing the particle-particle interaction. More and less sophisticated methods of accomplishing this give results with varying levels of accuracy. Chen and Sheng³³ have modeled fractal aggregates of gold nanoparticles using anisotropic polarizabilities that are enhanced along the axis that connects a given particle with its nearest neighbors. They have developed rigorous methods for calculating the polarizabilities of cylindrical particles in infinite one-dimensional chains, and comparably accurate means could be employed to calculate polarizabilities for spherical particles in finite three-dimensional chainlike structures. While particles in a fractal aggregate could be assigned particle-specific anisotropic renormalized polarizabilities according to the local structure, the model would lose accuracy if a lattice gas structure was imposed so as to allow for Fourier-space solutions. Markel and Shalaev³⁴ have adopted a method introduced by Singham and Bohren³⁵ in which the lattice on which the nanoparticles are arrayed is compressed to a lattice constant smaller than the particle diameter so that the coupled dipole interaction is enhanced to reflect higher-order interactions in an approximate fashion.

Materials composed of metal nanoparticles with dielectric coating layers, however, are promising candidates for direct application of the coupled-dipole modeling methods described here. If the exclusion layer is thick enough so that quadrupole interactions between the metal cores are negligible, the interactions become primarily long-ranged, and the dielectric properties of the material become less sensitive to details of the composite microstructure.

In a separate paper,²³ we use the method described here to model large arrays of gold nanospheres with the goal of illuminating the structural basis for changes in UV-visible optical properties observed upon DNA-directed nanoparticle assembly.

ACKNOWLEDGMENTS

We thank P. Flatau, B. Draine, and J. Goodman for use of their DDA codes which provided a basis for our coupled

nanosphere code and the machinery for efficient calculation of dipole polarizations. We thank D. Mackowski and M. Mishenko for use of their *T*-matrix codes which enabled us to calculate aggregate optical response at converged orders of multipole interaction. This research was supported by ARO Grant No. DAA G55-97-1-0133 and by NSF Grant No. CHE-9871903.

¹C. A. Mirkin, R. L. Letsinger, R. C. Mucic, and J. J. Storhoff, *Nature* (London) **382**, 607 (1996); J. J. Storhoff *et al.*, *J. Am. Chem. Soc.* **120**, 1959 (1998).

²D. A. Weitz and M. Oliveria, *Phys. Rev. Lett.* **52**, 1433 (1984); D. A. Weitz, J. S. Huang, M. Y. Lin, and J. Sung, *ibid.* **54**, 1416 (1985); C. Douketis, Z. Wang, T. L. Haslett, and M. Moskovits, *Phys. Rev. B* **51**, 11022 (1995).

³J. J. Storhoff, R. C. Mucic, C. A. Mirkin, and R. L. Letsinger (unpublished).

⁴A. A. Lazarides, J. J. Storhoff, C. A. Mirkin, and G. S. Schatz (unpublished).

⁵P. C. Ohara, D. V. Leff, J. R. Heath, and W. M. Gelbart, *Phys. Rev. Lett.* **75**, 3466 (1995); H. Mattoussi *et al.*, *Phys. Rev. B* **58**, 7850 (1998); S. Connolly, S. Fullam, B. Korgel, and D. Fitzmaurice, *J. Am. Chem. Soc.* **120**, 2969 (1998); R. L. Whetten *et al.*, *Acc. Chem. Res.* **32**, 397 (1999).

⁶J. J. Goodman, B. T. Draine, and P. J. Flateau, *Opt. Lett.* **16**, 1198 (1991).

⁷L. Tsang, C. Mandt, and K. H. Ding, *Opt. Lett.* **17**, 314 (1992).

⁸Y. M. Wang and W. C. Chew, in *IEEE Antennas and Propagation Society International Symposium* (Institute of Electrical and Electronics Engineers, New York, 1992), Vol. 3, pp. 929–932.

⁹G. Mie, *Ann. Phys. (Leipzig)* **25**, 377 (1908).

¹⁰C. F. Bohren and D. R. Huffman, *Absorption and Scattering of Light by Small Particles* (Wiley, New York, 1983), p.101.

¹¹W. T. Doyle, *Phys. Rev. B* **39**, 9852 (1989).

¹²W. A. Kraus and G. C. Schatz, *J. Chem. Phys.* **79**, 6130 (1983).

¹³B. T. Draine and J. Goodman, *Astrophys. J.* **405**, 685 (1993).

¹⁴B. T. Draine, *Astrophys. J.* **333**, 848 (1988).

¹⁵M. Petracic and G. Kuo-Petravic, *J. Comput. Phys.* **32**, 263 (1979).

¹⁶J. W. Cooley and J. W. Tukey, *Math. Comput.* **19**, 297 (1965).

¹⁷N. M. Brenner, *IEEE Trans. Audio Electroacoust.* **AU-17**, 128 (1969).

¹⁸For wavelengths up to and including 500 nm, the dielectric values of Johnson and Christy (Ref. 19) were used. For wavelengths longer than 500 nm, the dielectric values of Thèye (Ref. 20), as presented by Palik (Ref. 21) were used.

¹⁹P. B. Johnson and R. W. Christy, *Phys. Rev. B* **6**, 4370 (1972).

²⁰M.-L. Thèye, *Phys. Rev. B* **2**, 3060 (1970).

²¹D. W. Lynch and W. R. Hunter, in *Handbook of Optical Constants of Solids*, edited by E. D. Palik (Academic, New York, 1985), p. 294.

²²A. A. Lazarides and G. C. Schatz (unpublished).

²³A. A. Lazarides and G. C. Schatz, *J. Phys. Chem.* **104** (6) (in press).

²⁴D. W. Mackowski and M. I. Mishenko, *Appl. Opt.* **35**, 2182 (1996).

²⁵A. Liebsch and P. V. Gonzalez, *Phys. Rev. B* **29**, 6907 (1984).

²⁶S.-Y. Sheu, S. Kumar, and R. I. Cukier, *Phys. Rev. B* **42**, 1431 (1990).

²⁷F. Borghese, P. Denti, R. Saija, and O. I. Sindoni, *Nuovo Cimento* **13**, 1159 (1991).

²⁸W. Lamb, D. M. Wood, and N. W. Ashcroft, *Phys. Rev. B* **21**, 2248 (1980).

²⁹Francisco Claro, *Phys. Rev. B* **30**, 4989 (1984).

³⁰T. Jensen, L. Kelly, A. A. Lazarides, and G. C. Schatz, *J. Cluster Sci.* **10**, 295 (1999).

³¹A. F. Peterson, S. L. Ray, C. H. Chan, and R. Mitra, in *Application of Conjugate Gradient Method to Electromagnetics and Signal Processing*, edited by T. K. Sarkar (Elsevier, New York, 1991), Chap. 5.

³²T. Kozasa, J. Blum, and T. Mukai, *Astron. Astrophys.* **263**, 423 (1992); R. Stognienko, Th. Henning, and V. Ossenkopf, *ibid.* **296**, 797 (1995).

³³Z. Chen *et al.*, *Phys. Rev. B* **37**, 5232 (1988); Z. Chen and P. Sheng, *ibid.* **39**, 9816 (1989).

³⁴V. A. Markel *et al.*, *Phys. Rev. B* **53**, 2425 (1996).

³⁵S. B. Singham and C. F. Bohren, *J. Opt. Soc. Am. A* **5**, 1867 (1988).